Materials Science in Semiconductor Processing 37 (2015) 190–198

Contents lists available at ScienceDirect

Materials Science in Semiconductor Processing

journal homepage: www.elsevier.com/locate/mssp

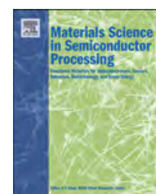

Formation of self-organized nano-surfaces on III–V semiconductors by low energy oxygen ion bombardment

A.G. Hernández*, Yu. Kudriavtsev, S. Gallardo, M. Avendaño, R. Asomoza

Departamento de Ingeniería Eléctrica-SEES, Centro de Investigación y de Estudios Avanzados del Instituto Politécnico Nacional, CINVESTAV-IPN, Av. IPN n. 2508, Col. San Pedro Zacatenco, D. F. C.P. 07360, Mexico

A R T I C L E I N F O

Available online 26 March 2015

Keywords:
Ion beam sputtering
GaAs
GaSb
InSb
Surface patterning

A B S T R A C T

Pattern formation on surfaces of III–V compound semiconductors GaAs, GaSb, and InSb by O_2^+ ion sputtering was studied. For GaAs, a ripple pattern was observed under a 2-keV primary beam energy for two ion fluences, i.e., 3.1×10^{18} ions/cm^2 and 5.4×10^{18} ions/cm^2. The pattern wavelengths were 175 nm and 200.2 nm. A bubble-like structure was observed on the GaSb surface bombarded with 1-keV and 2-keV oxygen ions. In the case of InSb, several pyramidal structures with sub-micrometer dimensions were observed when the ion energy was 1 keV. When the ion energy was increased to 2 keV, the pyramidal structures acquired micrometer dimensions and a ripple pattern with a wavelength of 246 nm was observed in the surrounding area.

© 2015 Elsevier Ltd. All rights reserved.

1. Introduction

A patterned surface is the surface that has been morphologically modified due to ion beam irradiation. Ion radiation leads to formation of well defined and highly oriented periodic structures on the surface. The patterns have different shapes and characteristics, they can be in the form of ripples, dots, cones, and pyramids [1]. Patterned surfaces have a variety of technological applications. For example, they are used in magnetic storage technology, in quantum devices, for enhancing the solar cell efficiency, for selective attachment of specific molecules, and for optoelectronic device fabrication [2–6]. Due to its simplicity, ion irradiation has been widely used for different solid materials [7].

The modification of surface topography is inherent to IBS processes, since the technique involves the removal of atoms from the surface. This can be inconvenient in the case of depth profiling analysis by secondary ion mass spectroscopy (SIMS) and other ion sputtering based techniques due to a degradation of the depth resolution caused by the formation of patterns on the eroded surface [8].

The goal of our work was to study ripple formation for the low-energy range, from 0.5 to 2 keV, corresponding to the typical depth profiling regime of the new generation of SIMS instruments. Special attention should be given in this case to changes in the surface morphology in the range of energies used for depth profiling since a smooth surface is preferable. The objects in our experiments were III–V compound semiconductors because of their diverse applications in optoelectronics and nanostructured system fabrication.

In order to explain the self-organization of the patterned surfaces obtained by ion beam sputtering, different theoretical models have been developed. By using the Sigmund transport theory of sputtering, Bradley and Harper showed that ripples were formed due to a curvature dependent sputter yield [9]. According to this model, ripple formation is a thermally activated self-diffusion process that dominates the IBS at sufficiently high temperatures and low fluxes. In general, sputter rippling

* Corresponding author.
E-mail address: ghernandez@cinvestav.mx (A.G. Hernández).

http://dx.doi.org/10.1016/j.mssp.2015.02.074
1369-8001/© 2015 Elsevier Ltd. All rights reserved.

models contain the surface curvature dependence which describes rippling as a competition between ion beam roughening/etching and surface diffusion and viscous flow relaxation [1]. As mentioned above, the HB model is limited by an elevated temperature and low ion fluences; nonlinear effects are neglected. Because of this, subsequent modifications to the linear model were necessary to explain the formation of dot and cone patterns and also the smoothing effect on the eroded surfaces.

The surface smoothing for small incidence angles and the transition from smooth to rippled surfaces that takes place when the angle of incidence increases for Si and Ge were described by Teichmann [10]. The authors presented an overview of the subsequent modifications to the HB linear model when the nonlinear terms were taken into account.

The dot pattern formation is explained when we take into account the nonlinear terms and the smoothing mechanisms, such as the viscous flow suggested in [11]. In order to obtain an adequate model to describe the dot pattern formation with a hexagonal array it is necessary to take into account the presence of an amorphized top surface layer in the two-dimensional Kuramoto-Sivashinsky equation. The numerical simulation of this equation leads to three different solutions: (1) for large values of damping factor α, a periodic hexagonal morphology arises; (2) when α decreases, the hexagonal states begin to oscillate, and (3) when α reduces further, the oscillations become large enough to generate a spatiotemporal chaotic state [12].

The formation of conical structures on the InP surface can be attributed to a difference in the sputtering yields of the semiconductor components [13]. As a consequence, atoms with a lower sputter yield are accumulated on the surfaces and act as impurities. The impurities originates the cone development as a nonequilibrium process in which structures are created and then destroyed by a prolonged sputtering.

Preparation of patterned surfaces is a complicated task because several experimental parameters of the sputtering process such as the ion type, the primary ion energy, the angle of incidence, the ion fluence, the target type, and the target temperature affect the pattern characteristics. A salient feature of our experiments was the use of oxygen as a primary ion. Actually, formation of ripple or dot patterns by using noble gases as primary ions, mainly Ar^+, is well known and there is a wide body of experimental data for sputtering with noble gases [14]. The references given in our paper (except [8]), report the results obtained for sputtering using Ne^+, Ar^+, Kr^+ and Xe^+ ions in the sub-keV energy range. Elst et al. [8], studied the ripple formation and its influence on the depth profile degradation by bombardment with oxygen ions with an energy of 8 keV.

2. Experimental procedure

In our study the IBS was performed by using oxygen ion sputtering of InSb, GaSb and GaAs. Different ion energies and ion fluences were used.

The samples approximately 1×1 cm^2 in size were cut from standard 2" wafers and cleaned in an ultrasonic bath with ethanol during five minutes. Then, after drying during 20 min, they were placed into a vacuum chamber (load-lock). The root-mean-square (RMS) roughness of the

Table 1
Characteristics of GaAs, GaSb and InSb surfaces bombarded with O_2^+ ions. The ion energy and the ion fluence were varied for each material. The RMS was strongly modified after the ion bombardment.

Target	*Energy [keV]*	*Ion fluence [ions/cm^2]*	*RMS roughness before IBS [nm]*	*RMS roughness after IBS [nm]*	*Description of the surface after IBS*
GaAs	0.5	1×10^{19}	0.5	2.2	Flattened surface
		5×10^{18}		1.8	Flattened surface
	1	6.2×10^{18}		3.2	Early stage of ripple pattern
		1.8×10^{18}		4.0	Early stage of ripple pattern
		1.5×10^{18}		2.3	Early stage of ripple pattern
	2	5.4×10^{18}		**4.9**	**Ripple pattern**
		3.1×10^{18}		**4.4**	**Ripple pattern**
GaSb	**0.5**	5×10^{18}	1.6	**5.3**	**Early stage of ripple patter**
		2.5×10^{18}		**5.2**	**Early stage of ripple patter**
	1	6.2×10^{18}		6.1	Bubble-like structures
		3.1×10^{18}		5.5	Bubble-like structures
	2	5.4×10^{18}		8.2	Bubble-like structures
		7.5×10^{18}		6.9	Bubble-like structures
		3.7×10^{18}		8.1	Bubble-like structures
InSb	0.5	2.5×10^{18}	4.7	8.4	Bubble-like structures
		1.2×10^{18}		1.5	Flattened surface
		6.2×10^{17}		5.1	Flattened surface
		4.2×10^{17}		5.2	Flattened surface
	1	6.2×10^{18}		7.1	Pyramidal structures
		3.1×10^{18}		9.6	Pyramidal structures
		1.0×10^{18}		6.1	Pyramidal structures
	2	1.5×10^{19}		**1.3**	**Pyramids and ripple pattern**
		7.5×10^{18}		**1.8**	**Pyramids and early stage of ripple pattern**
		3.7×10^{18}		5.5	**Pyramids**
		2.5×10^{18}		8.6	**Pyramids**

surface before ion irradiation was measured as 0.5 nm for GaAs, 1.6 nm for GaSb and 4.7 f or InSb.

Controlled ion irradiation was carried out at room temperature by O_2^+ ions with ion energies of 0.5, 1, and 2 keV using a TOF-SIMS-5 secondary ion mass spectrometer from ION-TOF. The ion bombardment was performed at a 45° incidence angle with a constant (for each ion energy) ion beam current and beam raster size and different sputtering times under ultra-high vacuum (UHV) conditions (the base pressure was $\sim 10^{-9}$ mbar).

After ion irradiation the surface morphology was investigated by atomic force microscopy (AFM) using a Solver Next instrument from NT-DMT. We used the so-called tapping mode to analyze the 3-D surface relief. All the measurements were conducted in air by using silicon tips with a tip curvature radius of about 35 nm. The AFM measurements were performed for different scan sizes from $2 \times 2\ \mu m^2$ to $50 \times 50\ \mu m^2$ with a resolution of 512×512 pixels and scanning frequency of 3 Hz. The surface roughness statistics and the characteristics of nano-patterns, i.e., regularity, wavelength, and amplitude, were analyzed.

3. Results and discussion

Table 1 shows the sputtering conditions used for each semiconductor and a brief description of the status of the surface after the IBS. All the measurements of the root-mean squares (RMSs) were analyzed.

3.1. GaAs

Fig. 1 shows the GaAs surface after O_2^+ ion irradiation with two different energies for ion fluence in almost the same. One can observe in images Fig. 1(a) and (b) the evolution of the surface until a ripple pattern is formed as the energy of the ion beam increases.

Image Fig. 1(a) shows the early stage of the ripple pattern produced by 1 keV ion sputtering. Under these experimental conditions the pattern was neither uniform nor orientated. It can be concluded from the results obtained that in the case of GaAs bombarded with oxygen ions the ripple pattern formation strongly depends on the beam energy.

Fig. 2 shows the GaAs surface sputtered by oxygen ions with energy of 1 keV and different ion fluences. As the fluence increases, a wave-like structure is observed. However, as cross sectional analysis shows, the structures formed are not periodic for any ion fluence used. A correspondent image analysis revealed many morphological irregularities on the surface. For low ion fluences, such as 1.5×10^{18} ions/cm^2, no tendency to the formation of a ripple pattern was observed. But as the ion fluence increased up to 1.8×10^{18} ions/cm^2, the early stage of the ripple pattern arose. On the other hand, a coarsening of the wave-like shapes was observed for an ion fluence of 6.2×10^{18} ions/cm^2. The coarsening behavior is not predicted by the HB theory. However, when the nonlinear terms are included, the ripple coarsening can be predicted by using the so-called hydrodynamic model [15].

When we increased the energy of the incident ion beam up to 2 keV a well-defined ripple pattern was observed. The HB theory predicts that the orientation of the pattern is determined by the direction of the ion beam, for angles close to the grazing incidence, the wave vector of the ripples is perpendicular to the beam direction [9]. In our case, at a 45° incidence angle, the wave vector of the ripple pattern is perpendicular to the ion beam direction. For this energy, an increase in the ion fluence leads to a ripple coarsening. Fig. 3 shows the 3D GaAs surface after irradiation with 2- keV O_2^+ ions for 3.1×10^{18} ions/cm^2 (a) and 5.4×10^{18} ions/cm^2 (b) fluences. For the first case, the ripple pattern wavelength was 175 nm, and for second case the corresponding wavelength was 200.2 nm. As the fluence increased, the surface roughness also increased from 4.4 to 4.9 nm. This behavior is

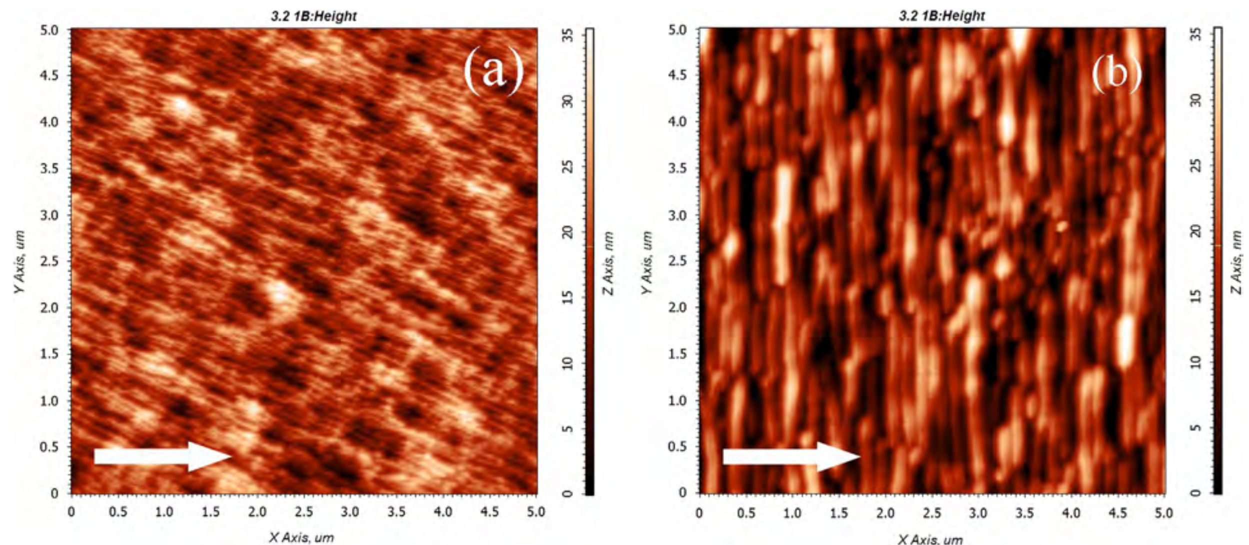

Fig. 1. $5 \times 5\ \mu m^2$ AFM images of GaAs bombarded with oxygen ions at 45° incidence angle and different ion beam energies: (a) 1 keV, ion fluence is 6.2×10^{18} ions/cm^2, (b) 2 keV, ion fluence is 5.4×10^{18} ions/cm^2. The white arrow indicates the direction of the incident ion beam.

Fig. 2. 2×2 μm^2 images of GaAs surfaces bombarded with O_2^+ ion beam, the ion energy remains constant at 1 keV and the ion fluence is different for each case: (a) 1.5×10^{18} ions/cm^2, (b) 1.8×10^{18} ions/cm^2, and (c) 6.2×10^{18} ions/cm^2. The white arrow indicates the direction of the ion beam at a 45° incidence angle.

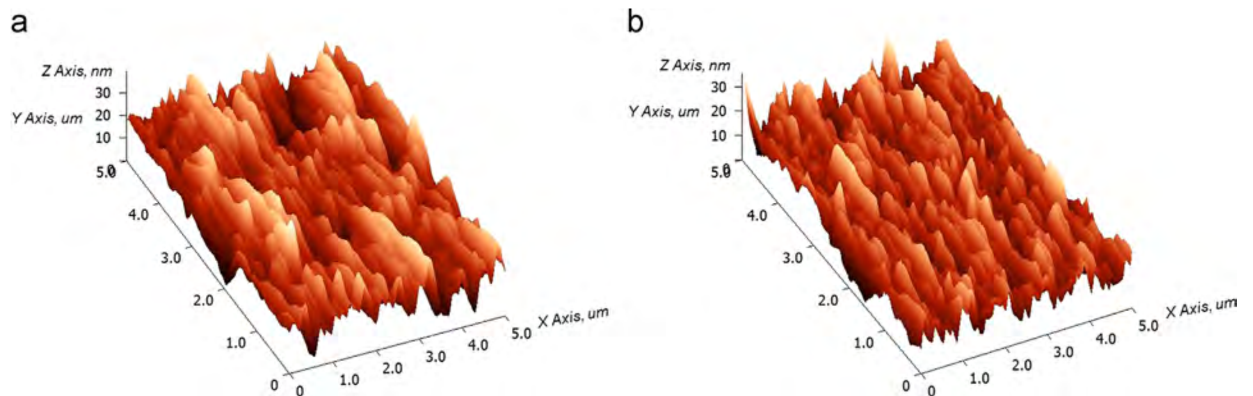

Fig. 3. 3D surfaces of GaAs after ion bombardment with oxygen ion beam at 45° incidence. The ion beam energy is 2 keV, ion fluences are 3.125×10^{18} ions/cm^2 (a) and 5.4×10^{18} ions/cm^2 (b). The images size is 5×5 μm^2.

consistent with the experimental results reported by Chan [14], who supposed that in some cases the ripple wavelength and surface roughness were found to increase with time according to a power law. This situation is not predicted by the BH instability theory and is attributed to the nonlinear effects [14].

In the case of ion irradiation with energy of 500 eV, no pattern formation was observed when the sputtering fluence was varied from 5×10^{18} ions/cm^2 to 1×10^{19} ions/cm^2.

The experimental results obtained for GaAs indicate that the wavelength of the ripple pattern varies linearly with energy and obeys the relation $l\sim\epsilon\cos\theta$, where θ is the angle of incidence [16]. In our experiment the strongly defined ripple pattern on the semiconductor surface occurred only for ion energy of 2 keV. For lower energies and different ion fluences, only the early stage of ripple pattern was observed for an energy beam of 1 keV.

The GaAs roughness prior to IBS was 0.5 nm, but it increased when the ion energy and the ion fluence increased. It can be seen from Table 1 that for an ion fluence of 5×10^{18} ions/cm^2 the roughness was 1.8 nm for the 500-eV ion beam energy. In contrast, the RMS roughness was as high as 4.9 nm for an ion energy of 2 keV with an ion fluence of 5.4×10^{18} ions/cm^2. Table 1 shows the increment of the RMS roughness as the energy beam increases.

According to the experimental results, the most convenient sputter regime for the GaAs depth profiling is the 500-eV

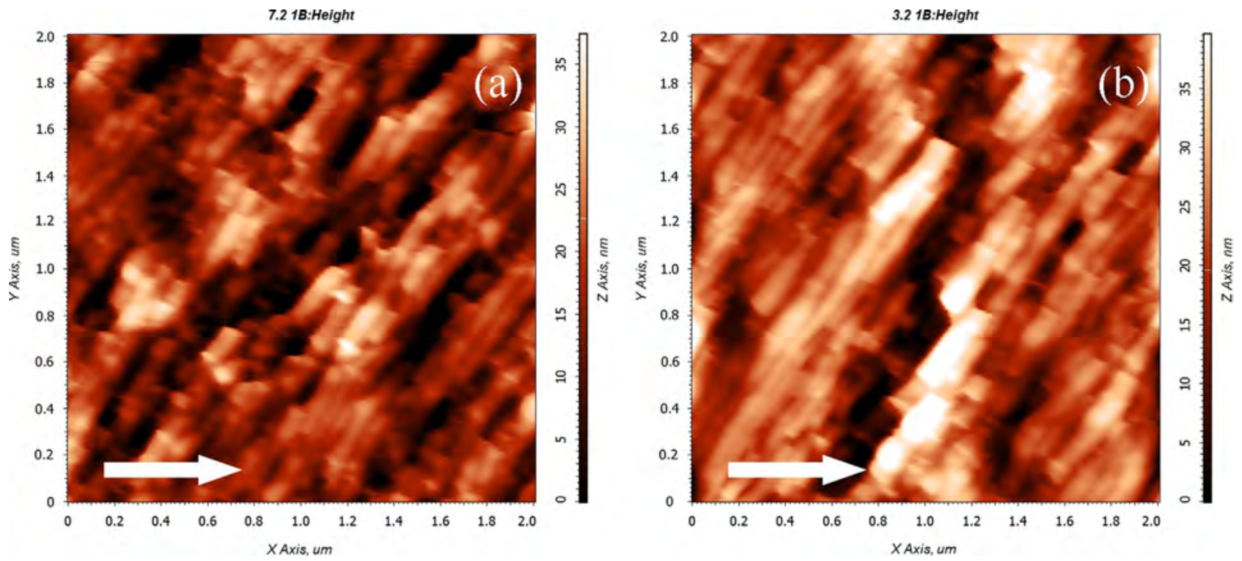

Fig. 4. 3D surface of GaSb after bombardment with 500-eV oxygen ions using different ion fluences: (a) 2.5×10^{18} ions/cm^2; the maximum height is 45 nm and (b) 5×10^{18} ions/cm^2, the maximum height is 70 nm. The angle of the incident ion beam is 45°. Image size is 5×5 μm^2.

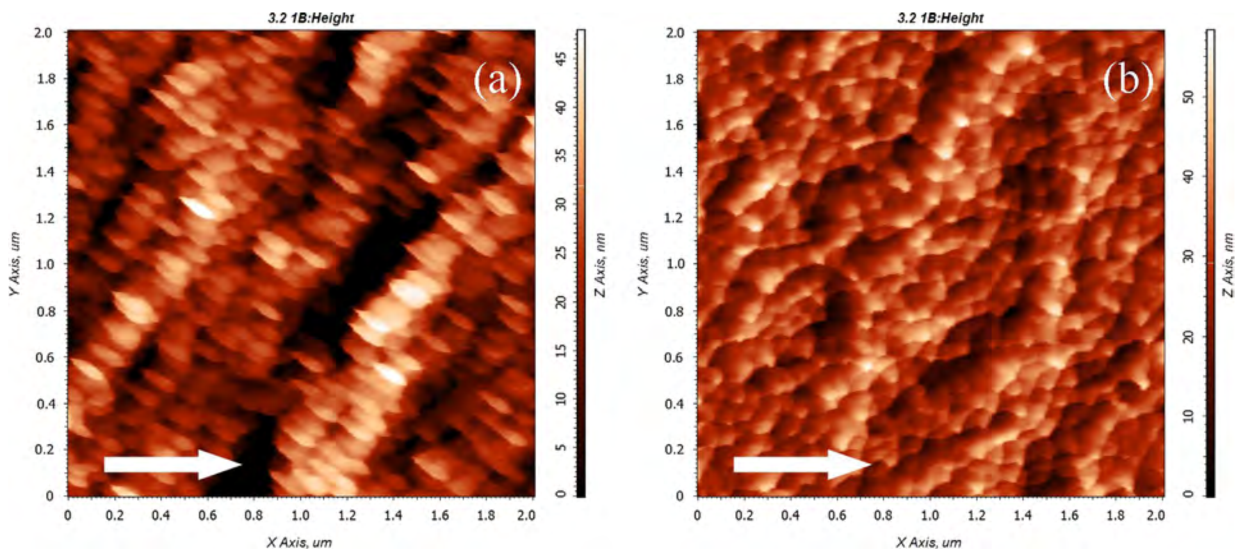

Fig. 5. 2×2 μm^2 AFM image of a GaSb surface after ion bombardment by O_2^+ ions at 45° incidence angle using different ion energies and ion fluences: (a) 1 keV, the ion fluence is 6.2×10^{18} and (b) 2 keV, the ion fluence is 5.4×10^{18}.

oxygen ion beam energy using a low fluence because no formation of structures on the surface occurs. For higher ion energies, sample rotation or a low temperature of the sample should be used to decrease the surface roughness induced by ion irradiation and to improve the SIMS depth resolution.

3.2. GaSb

For GaSb surface irradiated with the 500-eV ion energy, the early stage of the ripple pattern was observed. However, the obtained pattern was not uniform and the ripple wavelength varied over the entire irradiated area. Fig. 4 shows AFM images of the GaSb surface sputtered by 500-eV oxygen ions with two different ion fluences: 2.5×10^{18} ions/cm^2 (a) and 5×10^{18} ions/cm^2 (b). The pattern obtained a higher ion fluence is more uniform than that obtained at a lower ion fluence. The maximum surface peaks increase in their heights from 45 nm to 70 nm as the ion fluence increases from 2.5×10^{18} ions/cm^2 to 5×10^{18} ions/cm^2. For the ion fluence of 5×10^{18} ions/cm^2, the early stage of the ripple pattern was observed along a specific direction oblique to the primary ion incidence.

Fig. 5 shows the GaSb surface after ion irradiation with O_2^+ ions at 1 keV (a) and 2 keV (b). As the bombardment energy increases, a tendency to form bubble-like structures arises. As the ion fluence increases a stronger modification of the morphology was observed on GaSb surface after the 1-keV oxygen irradiation.

Fig. 6 shows the irradiated surface of GaSb for ion fluences of 3.1×10^{18} ions/cm^2 (a) and 6.2×10^{18} ions/cm^2 (b). The average sizes of the bubble-like structures are 77.7 nm and 99.5 nm. A coarsening of these structures was observed when the ion fluence increased. This behavior agrees with the results obtained by Fackso et al. [11], where a dot pattern coarsening was observed when the ion fluence increased. Nevertheless, our structures are not uniform and do not display a periodicity. However, it is interesting that after sputtering with 1- and 2-keV ion energies, the GaSb surfaces exhibited bubble-like structures, similarly to the work reported by Facksо, where a highly orientated dot pattern with a hexagonal symmetry was obtained by Ar^+ ion bombardment with a 420-eV energy under a normal incidence.

Table 1 shows that for the 0.5 and 1 keV ion energies the roughness increases with increasing ion fluence. In the case of the 2-keV ion energy, the roughness decreases from 8.1 to 6.9 as the sputter time increases. This result is in agreement with the formation kinetics of quantum dots (QDs) in the longer sputter time, which shows that the roughness reaches a maximum and decreases slightly to a steady-state value [14].

In the case of the GaSb ion bombardment, the early stage of ripple pattern was observed only for the 500-eV beam. As one can see from Fig. 4, the material does not agglomerate in a bubble-like structure as in the case of the structures obtained by using 1-keV and 2-keV beams. Allmers et al. [17] studied the transition from a bubble-like to a ripple formation on GaSb and revealed that there was a critical angle for this transition. Under their experimental conditions (argon ion beam sputtering with the 3-keV ion energy) the authors found that at the incidence angles close to the normal to the surface, the bubble-like pattern arose after IBS. However, if the incidence angles were in the range between 30° and 50°, a ripple pattern was observed for the same ion energy and fluence. This behavior does not agree with our experiments, i.e., formation of a bubble-like structure in the case of sputtering at a 45° incidence angle. We believe that this is due to the differences in the experimental parameters (ion type and energy). A deeper investigation is necessary in order to determine the influence of the angle of incidence on the pattern formation, in particular, on the QDs formation on the sputtered surface.

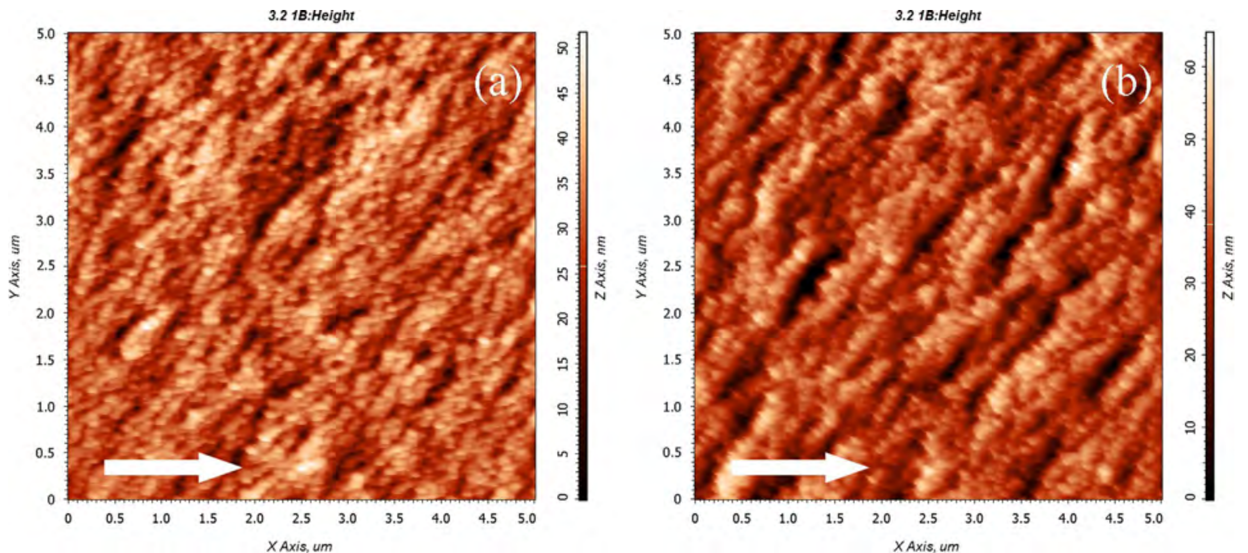

Fig. 6. 5×5 μm^2 AFM images of eroded GaSb by 1-keV oxygen ions for different ion fluences: 3.1×10^{18} ions/cm^2 (a) and 6.2×10^{18} ions/cm^2 (b). The angle of incidence is 45°. The white arrow shows the ion beam direction.

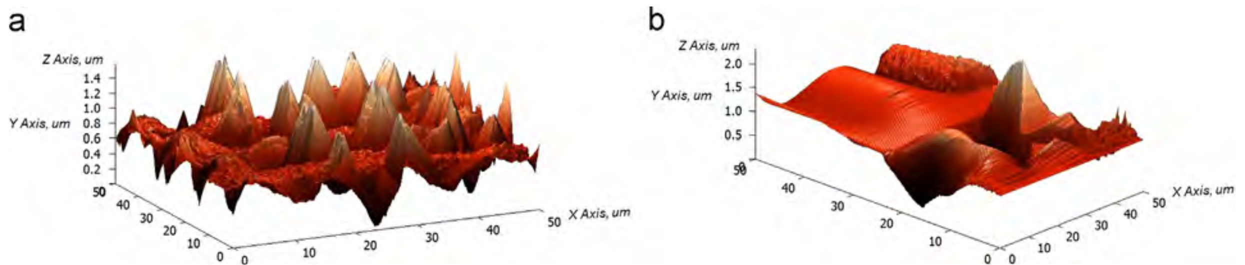

Fig. 7. 3D surface of InSb after ion irradiation with O_2^+ ions. The angle of incidence is 45° and the ion energy is 2 keV. Sputtering fluence is: 3.7×10^{18} ions/cm² (a) and 1.5×10^{19} ions/cm² (b). Image size is $50 \times 50 \times 5$ μm³.

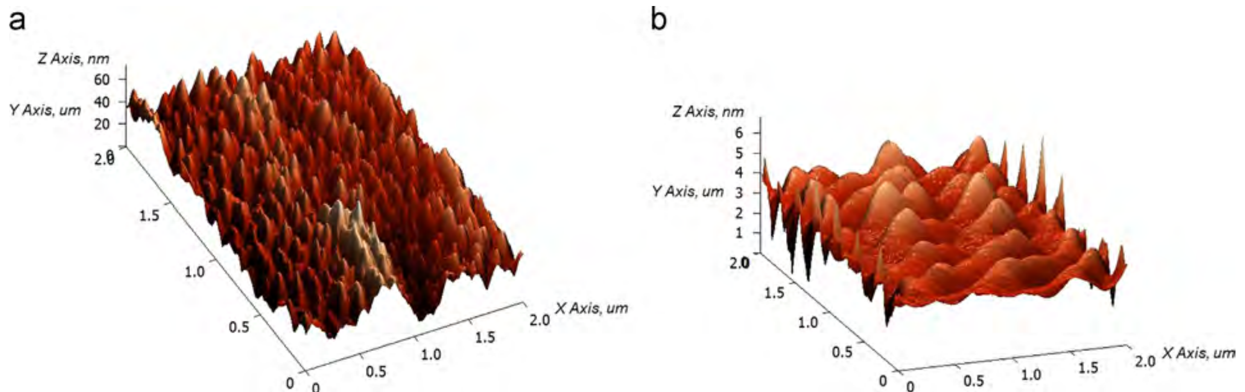

Fig. 8. 2×2 μm² micrographics in 3D of InSb surface after ion bombardment at a 45° incidence angle using a 2 keV oxygen ion beam at ion fluences 2.5×10^{18} ions/cm² (a) and 1.5×10^{19} ions/cm² (b).

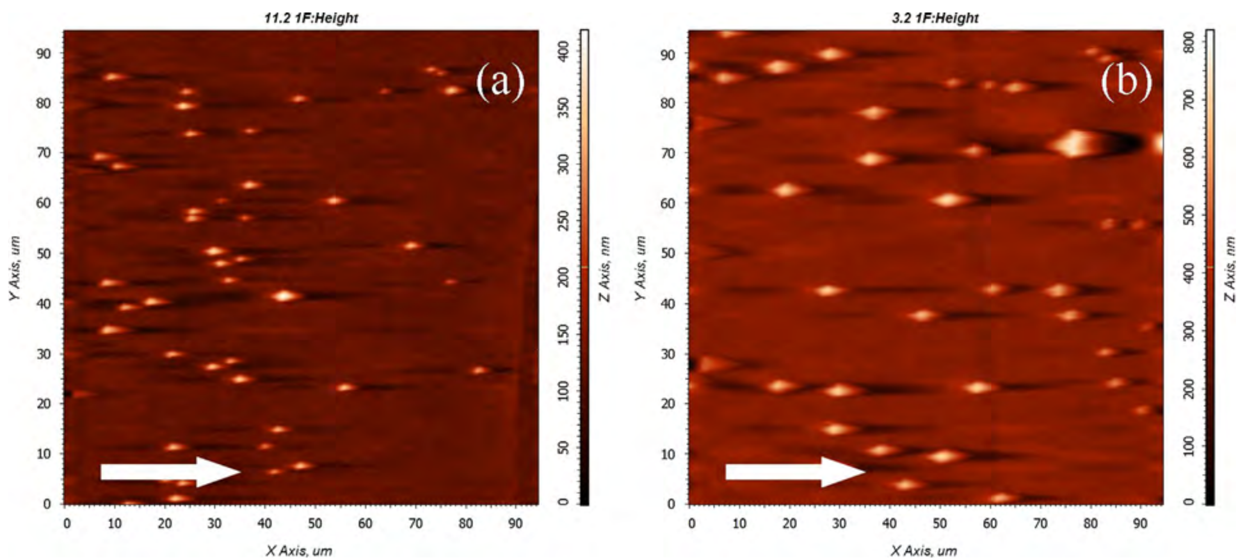

Fig. 9. AFM micrographics of InSb bombarded with oxygen ions. The angle of incidence is 45°, the ion beam energy is 1 keV. The ion fluence is: 3.1×10^{18} ions/cm² (a) and 6.2×10^{18} ions/cm² (b). Image size is 94.6×94.6 μm².

In general, the RMS of the bombarded GaSb surfaces increases with the ion beam energy. For the 500-eV ion energy the RMS roughness was 5.3 nm, in contrast to the RMS roughness for the 2-keV ion energy the maximum value of which was found to be 8.2 nm (see Table 1).

3.3. InSb

The InSb surfaces irradiated with the 2-keV and 1-keV energies exhibited several surface structures with pyramidal shape having nano- and micro-metric dimensions. The

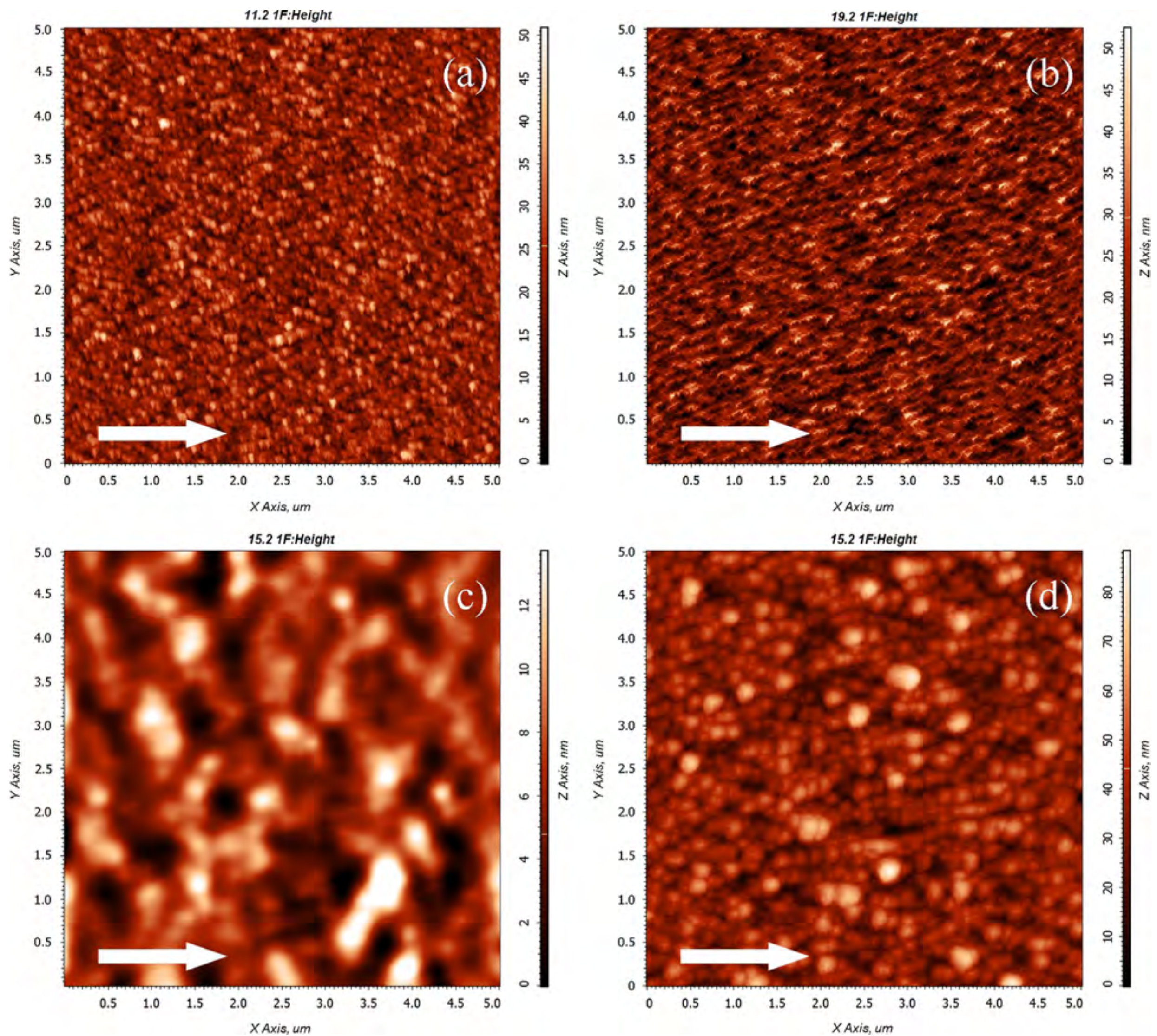

Fig. 10. AFM images, showing a sequence of the evolution of InSb surface topography with increasing the ion fluence: (a) 4.2×10^{17} ions/cm^2 (b) 6.2×10^{17} ions/cm^2 (c) 1.2×10^{18} ions/cm^2 (d) 2.5×10^{18} ions/cm^2. The ion energy is 500 eV and the angle of incidence is 45°. The images size is 5×5 μm^2.

structures were observed for all the ion fluences employed (Table 1). A strong modification of the original surface was also observed in the ***spaces*** between the pyramidal structures. The distance between the pyramids increased with the ion fluence in the case the energy was constant. Fig. 7 shows the pyramidal shapes obtained after ion bombardment using the 2-keV ion energy and different ion fluences: 3.7×10^{18} ions/cm^2 (a) and 1.5×10^{19} ions/cm^2 (b). In the first case many pyramids were observed in an area of 50×50 μm^2. As the ion fluence increased, the number of pyramids reduced but the heights of the pyramids increased. The maximum pyramid height obtained was found to be almost 2 μm for an ion fluence of 1.5×10^{19} ions/cm^2.

Fig. 8 shows the surface area between pyramids formed at the 2-keV oxygen ion sputtering with 2.5×10^{18} ions/cm^2 (a) and 1.5×10^{19} ions/cm^2 ion fluences (b). For the first ion fluence, the ripple pattern is in the early stage of formation. However, as the ion fluence increases, a highly oriented ripple pattern arises: the ripple pattern wavelength is 246 nm and the amplitude is less than 10 nm.

Fig. 9 shows the InSb surface after the 1-keV oxygen ion beam sputtering. The pyramidal structures with nanometric dimensions were observed for the ion fluences of 3.1×10^{18} ions/cm^2 (a) and 6.2×10^{18} ions/cm^2 (b). The behavior of these structures was similar to the behaviors of the structures obtained at the 2-keV beam energy, an increase in the ion fluence led to an increase in the pyramid height and the distance between pyramids. In contrast to the 2-keV ion sputtering reported above, no formation of a secondary pattern between pyramidal structures was observed for the 1-keV ion beam sputtering.

In the case of the 500-eV bombardment energy, no pyramidal structures were found for the ion fluences employed. Fig. 10 shows the InSb surfaces after

ion bombardment with the following ion fluences: 4.2×10^{17} ions/cm^2 (a), 6.2×10^{17} ions/cm^2 (b), 1.2×10^{18} ions/cm^2 (c), and 2.5×10^{18} ions/cm^2 (d). The surface is characterized by formation of bubble-like structures, and the size of these structures increases with increasing ion fluence.

According to our experimental results, the pyramid height varied from hundreds of nanometers to micrometers when the ion energy varied from 1 keV to 2 keV. The roughness analysis for InSb is complicated because of formation of a secondary pattern for the ion energy of 2 keV. Allmers [17] found that the impurities acted as nucleation centers for the formation of different nano-structures, such as pyramids and cones. Mac Laren and co-workers reported [13] that conical structures arose on InP surfaces after IBS using argon ions. The authors attributed the formation of In clusters on InP surfaces to a preferential P sputtering. This led to indium enrichment of the surface, then In atoms agglomerated into clusters due to surface diffusion. Due to the fourfold difference in the sputter rates of In and InP, the subsequent selective sputtering of InP resulted in the formation of cone-like surface structures.

We performed a Monte-Carlo simulation by using the TRIM-2010 code for InSb for the experimental parameters used in this study: oxygen is a primary ion beam, 1 keV is the ion energy and 45° is the angle of incidence. SRIM data indicate that there is no preferential sputtering for InSb target with formation of metal clusters. So, the mechanism of surface cluster formation due to preferential sputtering of one component [13] cannot be exploited to explain formation of pyramidal structures in the case of InSb. We estimated the sputtering yield (Y) of InSb and semiconductor components as

$$\gamma_{In}=2.25\ \text{particles/ion},\ \gamma_{Sb}=1.60\ \text{particles/ion},\ \gamma_{InSb}=1.58\ \text{particles/ion}$$

The sputter yields for InSb, In and Sb are close so there is no selective sputtering. As well there is no experimental confirmation about any relation between pyramidal (or cone) surface structures formation due to IBS, and any material structural features like defects or dislocations. So, in order to explain the experimentally observed morphology of InSb after IBS we can relate to effect of different low sputter impurities, intrinsic for this material or adsorbed from residual atmosphere [18]. Additional characterizations are required to confirm this hypothesis.

4. Conclusion

After ion irradiation of the III–V semiconductors with O_2^+ ions, patterned surfaces were observed on GaAs and InSb. So, the surface patterning is not exclusive of the ion bombardment with noble gases. For GaAs, the ripple pattern was observed for the 2-keV beam and it is wavelength depends on the ion fluence. On the other hand, for the irradiated surface of InSb the pyramid height was found to be directly proportional to the primary ion energy. Our computer code simulations have demonstrated that the pyramid formation cannot be explained by preferential sputtering of Sb (no In) with agglomeration of the enriched component and subsequent selective sputtering of the matrix surface discussed in the literature.

As mentioned above, the formation of dot, bubble, ripple and pyramidal structures results in a degradation of depth resolution of any SIMS depth profiling analysis. The experimental data obtained in this study can be used as a reference for the most convenient sputtering regime for depth profile analysis of the III–V semiconductor group commonly employed for device fabrication. In the case of GaAs and InSb, oxygen ion sputtering with an ion energy of 500 eV does not result in any pattern formation. On the contrary case, for the same energy the GaSb surface presents the early stage of ripple pattern if this energy is used. For a longer sputter time, as instance, the depth profiling of multilayer devices, the use of an ion beam with energy of 1 keV induces a modification of the morphology where the early stage of ripple pattern was observed in GaAs, bubble-like structures in GaSb and pyramids in InSb. Is this change in the surface morphology which is to be avoided in the study of depth profiling. Whereas for an ion beam energy of 2 keV a ripple pattern was observed on GaAs and a coarsening of the pyramidal structures in InSb, whilst for GaSb there was bubble-like pattern.

Acknowledgments

The authors would like to thank to the Mexican National Council for Science and Technology (CONACYT Reg. 271128) to supporting financially this work from the Project no. CB-2012/176179.

References

[1] J. Erlebacher, M.J. Aziz, E. Chason, M.B. Sinclair, J.A. Floro, Phys. Rev. Lett. 82 (11) (1999) 2330.
[2] J. Shen, J. Kischner, Surf. Sci. 500 (2002) 300.
[3] C.H. Sun, P. Jiang, B. Jiang, Appl. Phys. Lett. 92 (2008) 061112.
[4] B. Kasemo, Surf. Sci. 500 (2002) 656.
[5] A. Wellner, R.E. Palmer, J.G. Zheng, C.J. Kiely, K.W. Kolasinski, J. Appl. Phys. 91 (5) (2002) 3294.
[6] D. Datta, S.R. Bhattacharyya, T.K. Chini, M.K. Sanyal, Nucl. Instrum. Methods Phys. Res. B 193 (2002) 596.
[7] M.V.R. Murty, Surf. Sci. 500 (2002) 523.
[8] K. Elst, A. Adriaens, F. Adams, Int. J. Mass Spectrom. Ion Processes 171 (1997) 191.
[9] R.M. Bradley, J.M.E. Harper, J. Vac. Sci. Technol. A 6 (4) (1988) 2390.
[10] M. Teichmann, J. Lorbeer, B. Ziberi, F. Frost, B. Rauschenbach, New J. Phys. 15 (2013) 103029.
[11] S. Facsko, T. Dekorsy, C. Koerdt, C. Trappe, H. Kurz, A. Vogt, H.L. Hartnagel, Science 285 (1999) 5433. 1551.
[12] M. Paniconi, K.R. Elder, Phys. Rev E 56 (3) (1997) 2713.
[13] S.W. MacLaren, J.E. Baker, N.L. Finnegan, C.M. Loxton, J. Vac. Sci. Technol. A 10 (1992) 468.
[14] W.L. Chan, E. Chason, J. Appl, Phys. 101 (2007) 121301.
[15] J.M. García, M. Castro, R. Cuerno, Phys. Rev. Lett. 96 (2006) 086101.
[16] M.A. Makeev, R. Cuerno, A.L. Brarabási, Nucl. Instrum. Methods Phys. Res. B 197 (2002) 185.
[17] T. Allmers, M. Donath, G. Rangelov, J.Vac. Sci. Technol. B 24 (2) (2006) 582.
[18] K. Zhang, M. Brötzmann, H. Hofsäss, New J. Phys. 13 (2011) 013033.